

## Identification and Characterization of Potential Shear Transformation Zones in Metallic Glasses

Francesco Delogu\*

*Dipartimento di Ingegneria Chimica e Materiali, Università di Cagliari, piazza d'Armi, I-09123 Cagliari, Italy*  
(Received 23 January 2008; revised manuscript received 9 April 2008; published 27 June 2008)

The stability of local atomic configurations in a Ni-Zr metallic glass is studied by molecular dynamics. It is shown that individual atom displacements induce irreversible atomic rearrangements under different glass relaxation, temperature, and strain conditions. The number of regions with an unstable topology depends on the glass relaxation degree. Their time evolution is governed by thermal activation, the activation energy decreasing with elastic strain. It is also shown that unstable regions are located in correspondence of shear transformation zones operating under plastic deformation.

DOI: [10.1103/PhysRevLett.100.255901](https://doi.org/10.1103/PhysRevLett.100.255901)

PACS numbers: 66.10.-x, 61.43.Fs, 64.70.pe

Metallic glasses (MGs) are characterized by the absence of long-range structural order, which makes them exhibit physical and chemical properties different from those of their crystalline counterparts [1–3]. The lack of translational symmetry affects, in particular, the mechanical properties by suppressing the low-energy dislocation-mediated deformation mechanisms typical of crystalline phases [4,5]. Experimental and theoretical studies have shown indeed that MGs deform *via* relatively high-energy local atomic rearrangements according to the so-called Bulatov-Argon picture of microstructural shear banding [6–10], which predicts inelastic shear distortions localized in shear transformation zones (STZs) [4–12]. STZs consist of 10 to 100 atoms undergoing a transition, triggered by a volume redistribution, between two relatively low-energy configurations separated by an activation barrier [4–12]. Such an apparently simple definition hides a considerable complexity, and various fundamental questions on STZs are still open, including the connection between potential STZs and local structure as well as the size and shape of STZs and their activation mechanisms [4,5].

In the present work, the number and activation of STZs have been investigated by molecular dynamics simulations. Potential STZs have been identified by exploiting their instability with respect to small artificial displacements of individual atoms, which induce the irreversible rearrangement (IR) only of the species involved in a STZ. This method is reminiscent of the one employed in previous work to investigate local structural relaxation and plasticity of metallic and covalent network glasses [13]. It relies however on a perturbative approach rather than on potential energy minimization.

The present study was performed on a Ni<sub>50</sub>Zr<sub>50</sub> model glass. Calculations employed a semiempirical tight-binding (TB) potential based on a second-moment approximation to the electronic state density [14]. Although more refined force schemes could be used [15], it satisfactorily addresses the qualitative character of this work. Characteristic potential parameters were taken from literature [14,16]. Forces were computed within a cut-off radius of about 0.7 nm. Simulations were carried out within the *NPT*

ensemble with  $N$ , pressure  $P$ , and temperature  $T$  constant [17]. Equations of motion were solved with a fifth-order predictor-corrector algorithm [18] and a time step of 2 fs.

A Ni<sub>50</sub>Zr<sub>50</sub> glass of 65 536 atoms arranged in a volume  $V$  of  $13.3 \times 6.5 \times 13.3$  nm<sup>3</sup> was prepared by quenching the melt from 2000 to 300 K at a rate  $\dot{Q} = 2$  K ps<sup>-1</sup> and null pressure. Periodic boundary conditions (PBCs) were applied along  $x$ ,  $y$ , and  $z$  Cartesian directions. The glass transition, inferred by the Wendt-Abraham method [19], occurred at  $T_g \approx 1020$  K in accordance with previous work [20]. The glass was relaxed at 300 K for 40 ps. The Nosè thermostat was then removed to avoid perturbing the dynamics with stochastic effects and the system relaxed for 40 ps. The final configuration is indicated as  $C-I(300; 0; 2)$  to specify temperature, strain, and quenching rate of preparation.

The stability of local atomic arrangements in  $C-I(300; 0; 2)$  was studied by displacing any given atom from its position while leaving immobile the others. Displacements of length  $l_k = kl_m/10$  along 20 randomly selected directions were performed, being  $l_m$  the distance between the atom and the side of its Voronoi cell [21]. For each direction, the integer  $k$  was varied between 1 and 10 so that any given atom in  $C-I(300; 0; 2)$  was subjected to 200 independent displacements. After each displacement, the system was left free to evolve according to its dynamics for 20 ps. Any displacement introduces in the system an external perturbation the strength of which scales with  $l_k$ . In a perfect crystalline lattice, the displacement of any single atom within its Voronoi cell is not able to modify local atomic arrangements, and the displaced atom is pushed back to the center of the cell. In a glass, the stability against such perturbation depends instead on the local arrangement of neighbors.  $C-I(300; 0; 2)$  is left unaffected by roughly the 93% of displacements, as shown by the coincidence of 5-ps averaged atomic positions before and after the perturbation. In the other cases, IRs were instead identified by comparing initial and final average atomic positions  $r_{in}$  and  $r_{fin}$  within a sphere centered on the displaced atom and with radius  $r_3$ , being  $r_3$  the position of the third minimum of the global pair correlation function

(PCF) [18]. IRs were characterized by evaluating for each atom the difference  $\Delta r = |r_{\text{fin}} - r_{\text{in}}|/r_{\text{nn}}$ , where  $r_{\text{nn}}$  is the nearest-neighbors distance in the global PCF. The distribution  $p(\Delta r)$  of  $\Delta r$  is reported in Fig. 1 for both species involved in IRs and others. The two cases exhibit marked differences, although  $p(\Delta r)$  data superpose at small  $\Delta r$  values. IRs can be however distinguished from thermal motion because the roughly 10 to 20 atoms involved move collectively in about 1 ps. The IR onset is sensitive not to the direction but to the relative length  $l_k/l_m = k/10$  of displacements. The distribution  $p(k_{\text{min}})$  of the minimum values  $k_{\text{min}}$  above which IRs occur, shown in the inset, indicates that the average  $\langle k_{\text{min}} \rangle$  value amounts to about 7.1. About the 60% of atoms involved in a given IR are in turn able to induce an IR when displaced of a certain length  $l_k$ . In the 84% of such cases, the displacement of different atoms results in the same IR, with small differences between atomic positions due to thermal motion. It follows that IR atoms reside in regions with an unstable topology prone to a preferential structural evolution.

Similar results were obtained when individual atom displacements were performed in configurations C-II(300;0;2) and C-III(300;0;2), generated by evolving C-I(300;0;2) with no thermostat for time intervals  $\Delta t$  equal to 10 and 20 ns, respectively. The number  $N_{\text{IR}}$  of IRs in C-I(300;0;2), C-II(300;0;2), and C-III(300;0;2) was, respectively, of 421, 416, and 426. Such different values indicate that IRs can be thermally activated. IRs common to different configurations were identified on the basis of their position. The 94% of IRs in C-I(300;0;2) is found in C-II(300;0;2), the 92% of IRs in C-II(300;0;2) is found in C-III(300;0;2), and the 86% of IRs in C-I(300;0;2) is found in C-III(300;0;2). The average rate  $\dot{N}_{\text{IR}}$  of IR thermal activation, obtained by normalizing the number of activated IRs to volume  $V$  and time interval  $\Delta t$ , is then equal to about  $2.6 \mu\text{m}^{-3} \text{ns}^{-1}$ .

$N_{\text{IR}}$  and  $\dot{N}_{\text{IR}}$  are expected to depend, respectively, on quenching rate  $\dot{Q}$  and temperature. To address this point, other Ni<sub>50</sub>Zr<sub>50</sub> MGs were generated by quenching the initial 2000 K melt at different rates  $\dot{Q}$  and to different

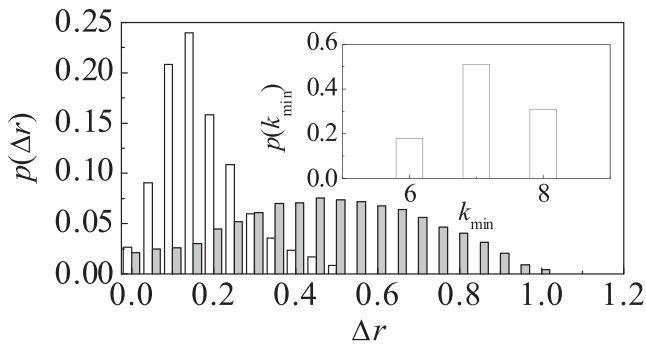


FIG. 1. The distribution  $p(\Delta r)$  of  $\Delta r$  values for species involved in IRs (gray bars) and others (hollow bars). The inset shows the distribution  $p(k_{\text{min}})$  of the minimum values  $k_{\text{min}}$  above which IRs take place. Data refer to C-I(300;0;2).

temperatures. C-I(300;0; $\dot{Q}$ ) systems were generated at 10, 50, and 100  $\text{K ps}^{-1}$ . Figure 2(a) shows that  $N_{\text{IR}}$  increases linearly with  $\dot{Q}$ , pointing out its intimate connection with the relaxation degree of the MG structure. C-I( $T$ ;0;2) systems were instead prepared by quenching the melt at 2  $\text{K ps}^{-1}$  to 500, 700, and 900 K.  $N_{\text{IR}}$  values are similar to the ones observed at 300 K. The Neperian logarithm of  $\dot{N}_{\text{IR}}$ ,  $\ln \dot{N}_{\text{IR}}$ , decreases instead linearly with  $T^{-1}$  as shown in Fig. 2(b). The underlying activation energy  $E_a \approx 27 \text{ kJ mol}^{-1}$  is significantly smaller than the one of 20–120  $RT_g$ ,  $R$  being the universal gas constant, generally expected on a semiempirical basis for STZs [4,9,13]. It is however remarkably close to the minimum STZ activation energy of about 33  $\text{kJ mol}^{-1}$  obtained for a Cu-Ti glass quenched at 0.1  $\text{K ps}^{-1}$  via a perturbation method similar to the one of the present work [22].

Aimed at studying how IRs are affected by shear, a configuration C-IV(300;0;2) was created. It is identical to C-I(300;0;2) except for the rigid reservoir regions 1.5 nm thick defined at the top and bottom of the simulation cell along the  $z$  Cartesian direction [11]. PBCs were applied along  $x$  and  $y$  ones. C-IV( $T$ ;0;2) systems were analogously created starting from the corresponding C-Is. The unstrained configurations (UCs) C-IV( $T$ ;0;2) were subjected to shear along the  $x$  Cartesian direction. Shearing was produced by imposing to reservoirs incremental displacements at a strain rate  $\dot{\epsilon}_x$  of about 27  $\text{ns}^{-1}$ . Similar results were obtained at 10 and 100  $\text{ns}^{-1}$ . Reservoirs were kept at constant distance, and no thermostat was

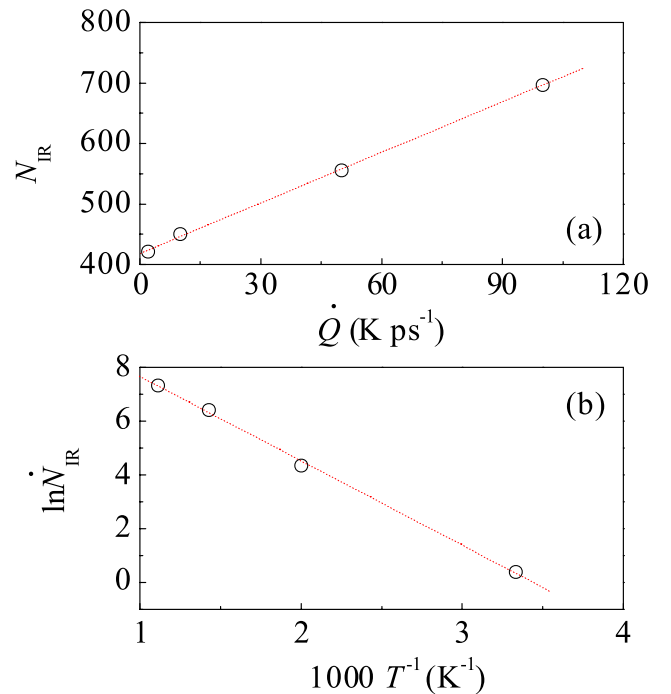


FIG. 2 (color online). (a) The number  $N_{\text{IR}}$  of IRs as a function of  $\dot{Q}$ . (b) The Neperian logarithm  $\ln \dot{N}_{\text{IR}}$  of the rate  $\dot{N}_{\text{IR}}$  of IR thermal activation as a function of  $T^{-1}$ . Best-fitted lines are also shown. Data refer to C-I( $T$ ;0;2) systems.

applied. Six elastically deformed configurations (EDCs), characterized by a strain  $\varepsilon_x$  between 0.02 and 0.09, were generated from each UC. The  $C\text{-IV}(T; \varepsilon_x; 2)$  EDCs were then subjected to individual atom displacements.

At  $\varepsilon_x$  values between 0.02 and 0.06, no significant plastic deformation has occurred, STZs did not massively operate, and most of the atoms experience elastic strain. Figure 3 shows that  $\langle k_{\min} \rangle$  undergoes a quadratic decrease with strain  $\varepsilon_x$ , whereas  $N_{\text{IR}}$  exhibits a quadratic increase. Elastic strain destabilizes then an increasing number of regions. IRs are insensitive to the direction of individual displacements. Additionally, both  $\langle k_{\min} \rangle$  and  $N_{\text{IR}}$  show a negligible temperature dependence.  $N_{\text{IR}}$  is instead slightly dependent on  $\dot{\varepsilon}_x$ , its values increasing roughly of the 10% at  $100 \text{ ns}^{-1}$ . As shown in Fig. 4(a), also for EDCs, the Neperian logarithm  $\ln \dot{N}_{\text{IR}}$  decreases linearly with  $T^{-1}$ . The activation energy  $E_{a,\varepsilon}$  obtained at each strain  $\varepsilon_x$  is reported in Fig. 4(b). At small  $\varepsilon_x$  values,  $E_{a,\varepsilon}$  decreases according to the equation  $E_{a,\varepsilon} = E_a - \gamma\varepsilon_x$ , being  $E_a \approx 27 \text{ kJ mol}^{-1}$  and  $\gamma \approx 207 \text{ kJ mol}^{-1}$ . When  $\varepsilon_x > 0.06$ ,  $E_{a,\varepsilon}$  exhibits instead a negative deviation from linearity, reaching an almost null value at the edge of plastic instability. At any temperature, IRs are therefore increasingly favored by the accumulation of elastic strain, in agreement with the strain-induced scenario for the modification of energy landscapes in glasses [23]. The linear relationship above provides further information. The term  $\gamma\varepsilon_x$  can be indeed written as  $\tau_x \Omega_{\text{act}}$  [24],  $\Omega_{\text{act}}$  being the average activation volume of IRs and  $\tau_x = \mu\varepsilon_x$  the shear stress along the  $x$  Cartesian direction, with  $\mu$  the shear modulus. For the  $\text{Ni}_{50}\text{Zr}_{50}$  MG investigated,  $\mu \approx 48 \text{ GPa}$  in rough agreement with experimental data [25]. It follows that  $\Omega_{\text{act}} \approx 7 \text{ \AA}^3$ , in agreement with the empirical estimate obtained from a colloidal glass [24]. It is now worth noting that both  $E_a$  and  $\Omega_{\text{act}}$  values are very close to the corresponding quantities for the low-energy diffusion mode in Ni-Zr MGs described in previous work [26]. These results suggest a connection between IRs and the scenario of inhomogeneous atomic

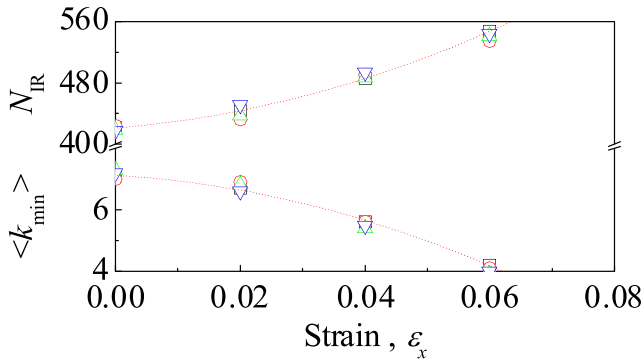


FIG. 3 (color online). The average  $\langle k_{\min} \rangle$  values and the number  $N_{\text{IR}}$  of IRs as a function of strain  $\varepsilon_x$ . Data refer to  $C\text{-I}(300; 0; 2)$  ( $\square$ ),  $C\text{-I}(300; 0; 2)$  ( $\circ$ ),  $C\text{-I}(300; 0; 2)$  ( $\triangle$ ), and  $C\text{-I}(300; 0; 2)$  ( $\nabla$ ) glasses. Quadratic curves are best-fitted on  $C\text{-I}(300; 0; 2)$  data.

mobility in MGs [27]. In addition,  $\Omega_{\text{act}}$  is much closer to the Ni atomic volume,  $\sim 12 \text{ \AA}^3$ , than to the Zr one,  $\sim 25 \text{ \AA}^3$ . This suggests in turn that the mobility of Ni atoms plays a major role, which provides a rationale for the fact that Ni atoms involved in IRs are roughly twice Zr ones.

IR positions in parent UCs and corresponding EDCs were compared *via* affine transformations. The probability  $\Gamma_{\text{IR}}$  that IR positions in UCs and EDCs coincide ranges from 83% at  $\varepsilon_x = 0.02$  to 75% at  $\varepsilon_x = 0.06$ . Differences can be ascribed to the onset of some IRs (IRs present in UCs and not in EDCs) or to the appearance of new IRs (IRs present in EDCs and not in UCs) during shearing. Roughly the same IRs operate then in UCs and EDCs at small  $\varepsilon_x$  values.  $\Gamma_{\text{IR}}$  drops however to 52%, 45%, and 38% at  $\varepsilon_x$  values of 0.07, 0.08, and 0.09, indicating the occurrence of significant atomic rearrangements during the deformation process.

Further insight into IRs was obtained from plastically deformed configurations (PDCs).  $C\text{-V}(T; \varepsilon_x; 2)$  PDCs were generated from  $C\text{-IV}(T; 0; 2)$  ones by shearing at the different temperatures  $T$  explored. Shearing was interrupted at  $\varepsilon_x$  values of 0.1, 0.15, and 0.2 and PDCs left free to evolve according to their dynamics for 10 ns. Following previous work [28], the atoms subjected to inelastic displacements

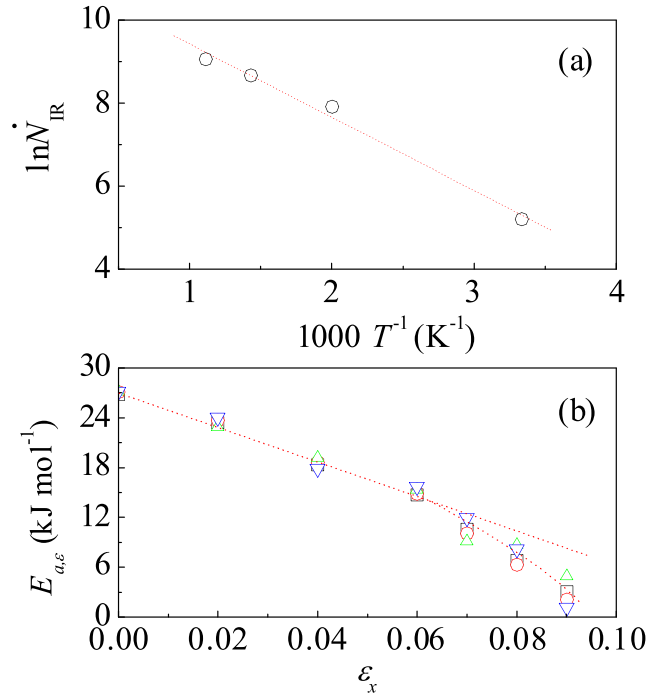


FIG. 4 (color online). (a) The Neperian logarithm  $\ln \dot{N}_{\text{IR}}$  of the IR rate of change  $\dot{N}_{\text{IR}}$  as a function of  $T^{-1}$  for  $C\text{-IV}(300; 0.06; 2)$ . The best-fitted line is also shown. (b) The IR activation energy  $E_{a,\varepsilon}$  as a function of strain  $\varepsilon_x$ . Data refer to  $C\text{-IV}(300; \varepsilon_x; 2)$  ( $\square$ ),  $C\text{-IV}(500; \varepsilon_x; 2)$  ( $\circ$ ),  $C\text{-IV}(700; \varepsilon_x; 2)$  ( $\triangle$ ), and  $C\text{-IV}(900; \varepsilon_x; 2)$  ( $\nabla$ ). The dotted line has been best-fitted on  $C\text{-IV}(300; \varepsilon_x; 2)$  ( $\square$ ) values. The dotted curve is a guide to the eyes.

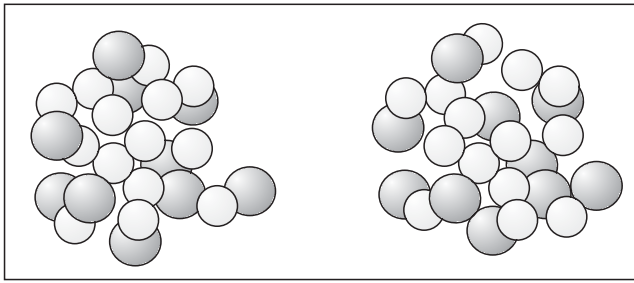


FIG. 5. A STZ before (left) and after (right) operation. Data refer to  $C$ -IV(500; 0.06; 2). Dark and light gray indicate, respectively, Zr and Ni atoms.

in STZs operating under shear were identified by the deviatoric participation ratio. This corresponds to the fraction of atoms with local deviatoric strain larger than the nominal strain  $\epsilon_x$  [28]. A typical STZ is shown in Fig. 5. The affine transformation of UCs into PDCs indicates that STZs roughly operate in the same regions of previously identified IRs, which can be thus tentatively regarded as potential STZs. However, IRs occurring in UCs and EDCs are different from STZs observed in PDCs. STZs have indeed catalytic effects, generally favoring successive STZs in the neighborhood, not observed in IRs.

Once shearing was interrupted and the  $C$ -V( $T$ ;  $\epsilon_x$ ; 2) PDCs relaxed, the rate  $\dot{N}_{\text{IR}}$  of IR thermal activation in PDCs was estimated over a time interval  $\Delta t$  of 10 ns.  $\dot{N}_{\text{IR}}$  exhibits again an exponential dependence on  $T$  with activation energy  $E_a$  of about 31, 26, and 29 kJ mol<sup>-1</sup> for PDCs with final strain  $\epsilon_x$ , respectively, of 0.1, 0.15, and 0.2. IRs in UCs and relaxed PDCs have then roughly the same activation energy.

In summary, relaxed MGs have been perturbed by displacing individual atoms to investigate the stability of local atomic configurations at different temperatures and strains. In about 7% of cases, perturbations trigger IRs involving about 20 atoms. Being the temperature constant, the higher the melt quenching rate  $\dot{Q}$ , the larger the number  $N_{\text{IR}}$  of IRs observed. Because of thermal activation, the IRs common to successive configurations decrease with time at a rate  $\dot{N}_{\text{IR}}$  that increases with temperature. The underlying activation energy amounts roughly to 27 kJ mol<sup>-1</sup> in UCs, but almost vanishes in EDCs close to yield point. IRs taking place in relaxed PDCs exhibit however the same activation energy of IRs occurring in UCs. Finally, STZs and IRs involve roughly the same regions and the thermal activation of IRs modifies number and position of STZs under shearing. IRs can be then regarded as potential STZs. These findings lend support to previous studies pointing out a correspondence between regions undergoing local structural relaxations under thermal activation and under shear [13]. In particular, the quadratic dependence of  $\langle k_{\text{min}} \rangle$  and  $N_{\text{IR}}$  on elastic strain  $\epsilon_x$  seems somewhat analogous to the one of the Gibbs activation energy of unit relaxation events in covalent network glasses at 0 K [13].

Financial support has been given by the University of Cagliari. A. Ermini, ExtraInformatica s.r.l., is gratefully acknowledged for his kind assistance.

\*delogu@dicm.unica.it

- [1] A. Inoue, *Acta Mater.* **48**, 279 (2000).
- [2] W.L. Johnson, *J. Met.* **54**, 40 (2002).
- [3] A.L. Greer and E. Ma, *MRS Bull.* **32**, 611 (2007).
- [4] C.A. Schuh, T.C. Hufnagel, and U. Ramamurty, *Acta Mater.* **55**, 4067 (2007).
- [5] A.R. Yavari, J.J. Lewandowski, and J. Eckert, *MRS Bull.* **32**, 611 (2007).
- [6] A.S. Argon and H.Y. Kuo, *Mater. Sci. Eng.* **39**, 101 (1979); A.S. Argon, *J. Phys. Chem. Solids* **43**, 945 (1982); V.V. Bulatov and A.S. Argon, *Model. Simul. Mater. Sci. Eng.* **2**, 167 (1994); **2**, 185 (1994); **2**, 203 (1994).
- [7] M.L. Falk and J.S. Langer, *Phys. Rev. E* **57**, 7192 (1998); J.S. Langer, *Phys. Rev. E* **64**, 011504 (2001); J.S. Langer, *Scr. Mater.* **54**, 375 (2006); M.L. Manning, J.S. Langer, and J.M. Carlson, *Phys. Rev. E* **76**, 056106 (2007).
- [8] A. Lemaitre, *Phys. Rev. Lett.* **89**, 195503 (2002).
- [9] M.L. Falk, *Phys. Rev. B* **60**, 7062 (1999); Y. Shi and M.L. Falk, *Phys. Rev. Lett.* **95**, 095502 (2005); Y. Shi, M.B. Katz, H. Li, and M. Falk, *Phys. Rev. Lett.* **98**, 185505 (2007).
- [10] C.A. Schuh and A.C. Lund, *Nat. Mater.* **2**, 449 (2003); A.C. Lund and C.A. Schuh, *Acta Mater.* **51**, 5399 (2003).
- [11] Q.-K. Li and M. Li, *Appl. Phys. Lett.* **88**, 241903 (2006).
- [12] E.A. Jagla, *Phys. Rev. E* **76**, 046119 (2007).
- [13] D. Deng and A.S. Argon, *Acta Metall.* **34**, 2011 (1986); **34**, 2025 (1986); M.J. Demkowicz and A.S. Argon, *Phys. Rev. Lett.* **93**, 025505 (2004); M.J. Demkowicz and A.S. Argon, *Phys. Rev. B* **72**, 245206 (2005); A.S. Argon and M.J. Demkowicz, *Philos. Mag.* **86**, 4153 (2006).
- [14] F. Cleri and V. Rosato, *Phys. Rev. B* **48**, 22 (1993).
- [15] I. Ladadwa and H. Teichler, *Phys. Rev. E* **73**, 031501 (2006).
- [16] C. Massobrio, V. Pontikis, and G. Martin, *Phys. Rev. Lett.* **62**, 1142 (1989).
- [17] H.C. Andersen, *J. Chem. Phys.* **72**, 2384 (1980); S. Nosé, *J. Chem. Phys.* **81**, 511 (1984).
- [18] M.P. Allen and D. Tildesley, *Computer Simulation of Liquids* (Clarendon Press, Oxford, 1987).
- [19] H.R. Wendt and F.F. Abraham, *Phys. Rev. Lett.* **41**, 1244 (1978).
- [20] H. Teichler, *Phys. Rev. B* **59**, 8473 (1999).
- [21] J.L. Finney, *Proc. R. Soc. A* **319**, 495 (1970).
- [22] S.G. Mayr, *Phys. Rev. Lett.* **97**, 195501 (2006).
- [23] D.J. Lacks, *Phys. Rev. Lett.* **87**, 225502 (2001).
- [24] P. Schall, D.A. Weitz, and F. Spaepen, *Science* **318**, 1895 (2007).
- [25] J.B. Rubin and R.B. Schwarz, *Phys. Rev. B* **50**, 795 (1994).
- [26] H. Teichler, *J. Non-Cryst. Solids* **293–295**, 339 (2001).
- [27] C. Donati *et al.*, *Phys. Rev. Lett.* **80**, 2338 (1998).
- [28] Y. Shi and M.L. Falk, *Phys. Rev. B* **73**, 214201 (2006).